*Bulletin of Pure and Applied Science*
*Physics, Vol.42D No.2S (Special Issue)*
*NCAEST-2023 P.65-77*
*Original Research Article*

*Print version ISSN 0970 6569*
*Online version ISSN 2320 3218*
*DOI: 10.62427/bpas.2023.42D.2S.9*
*Available online at www.bpasjournals.com*

# Micro Structural and Magnetic Properties of Nano Phase Iron- Doped Stannic Oxide Semiconductor Synthesized For Spintronics Applications

**[1]Sujeet Kumar, [2]Monalisa, [3]B.C. Rai*and [4]N.A. Karimi**

**Author's Affiliations:** [1,3]Department of Physics, College of Commerce Arts and Science, Patliputra University, Patna, Bihar 800020, India
[2]M.Tech, Nanoscience and Nanotechnology Centre, A. K. University, Patna, Bihar 800001, India
[4]B. N. College, Patna University, Patna, Bihar 800005, India

***Corresponding author:** **B.C. Rai**
Department of Physics, College of Commerce Arts and Science, Patliputra University, Patna, Bihar 800020, India
E-mail: bcraiphy@gmail.com

**ABSTRACT** Exploiting spin degree of freedom of charged carriers is a potential research field of future devices using spin current and externally controlled spin states in microchips. In this field, oxide hosts dilute doped by magnetic impurities (dilute magnetic semiconductor) promise development of the new form of electronics popular as spintronics. In this work, we report synthesis of iron doped stannic oxide, its microstructure and magnetic properties in nano phase. The samples are synthesized by chemical route of co-precipitation using magnetically stired aqueous solution of penta hydrate stannic chloride and tetra hydrate ferrous chloride with aqueous ammonia added drop wise till precipitation at $35^{O}$ C and the precipitates dried at $120^{o}$C in vacuum oven. Characterization of samples $Sn_{1-x}Fe_xO_2$ (x=0.00, 0.02, 0.04, 0.06, 0.08) by non-invasive X- ray diffraction and VSM techniques, indicated a particle size of 3nm, tetragonal unit cells having strained parameters that depended on concentration. The micro-strain and magnetic properties exhibit correlation.

**KEYWORDS** Iron doped stannic oxide; Micro-strain; Tetragonal unit cells.

**How to cite this article:** Kumar S., Monalisa, Rai B.C. and Karimi N.A. (2023). Microstructural and Magnetic Properties of Nano Phase Iron- Doped Stannic Oxide Semiconductor Synthesized For Spintronics Applications. *Bulletin of Pure and Applied Sciences- Physics,* 42D (2 Special Issue), 65-77.

## 1. INTRODUCTION

The microelectronics devices today utilize electric charge of electrons and holes without any consideration of their spins. The potential of spin can be used in new electronic devices encompassing a new field called spintronics (Zutic, Fabian and Sarma, 2004). Ever since Gordon Moore observed that the number of transistors per wafer would double every two years for improving microelectronic performance and industrial profitability (Moore, 1965) research on miniaturization of devices has gained focus all over the world. But that leads to higher power consumption, leakage and constant refreshing. In this grave situation, magnetic semiconductors pose a way out by their potential of remembering their spin states without any refresh, integration of logic and storage process without need of booting and low power requirement for spin manipulations. Metallic magnetic systems are used in hard disk

drives and read-write heads, but semiconducting environment imparts new functionality (Dattaand and Das, 1990). Magnetic semiconductor can facilitate injection of spin current into a nonmagnetic semiconductor, thus joining spin-based device to current devices (Rai et al., 2016). A semiconductor can be made magnetic by generating unbalanced spins or by substituting an impurity having a net spin (Ohno, 1998).

Magnetic transition metals (TM) taken in very small amount are suitable do pants to produce what is known as dilute magnetic semiconductors (DMS). Hosts of As, N formed IIIV systems such as (Ga,Mn) As, (In, Mn) As, (Ga, Mn) N, exhibited ferromagnetism with relatively well known mechanism of coupling of impurity magnetic moment with itinerant charge carriers (Jungwirth et al., 2006; Munekata et al., 1989; Ohno et al., 1992; Sasaki, 2002). However, the ferromagnetism was lost above a temperature (highest value 173 K) much below the room temperature. Several other systems were studied and mean- field Zener model predicted that this temperature could be elevated above room temperature by suitable choices of hosts, carrier concentration and the type and density of magnetic ion doped (Diett et al., 2000). Recently, wide band gap oxide based systems such as oxides of titanium, zinc and tin (Matsumoto et al., 2001; Ueda et al., 2001; Ogale et al., 2003; Janisch et al.,2005) have attracted attention due to their diverse optical and electrical behavior suited to devices. Intensive experimental exploration have so far produced diverse results ranging from non-ferromagnetic to ferromagnetic with various transition temperatures (Fukumura, 2005, Calderon & Sarma, 2007). In oxide based systems, carriers originate from oxygen vacancies as shallow donors while in III-V systems, these come from magnetic ions acting as donors or acceptors. At higher temperatures, thermally excited carriers also participate in ordering. Some results favor magnetism originating from magnetic clusters. Percolation of magnetic polar on sat lower temperatures and RKKY type origin at higher temperature are also used to understand magnetism (Liu & Wang, 2020). It appears that the re-exist various competing and complementing mechanisms specific to materials and methods of synthesis. Exclusive evidences of various mechanisms remain open under research. A synthesis product must therefore be analyzed for intrinsic or extrinsic origin of its magnetic and electric behavior, and possible micro-structural effects.

Tinoxide is a wide band gap (3.6eVinbulk) transparent and chemically stable semiconducting materials suitable to solar cell, gas sensing, catalytic and spintronics applications. It can be synthesized by various methods such as spray pyrolysis or flame spray synthesis (Sahm et al., 2004) laser removal process (Lu et al., 2006), mini arc plasma (Fujihara et al., 2004), hydrothermal (Shaikh et al., 2018 & Bhagwatet al., 2003), amorphous citrate route (Gnanam & Rajendram, 2010), wet chemical method (Li et al., 2002), solid state reaction (Hench & West, 1990), sol-gel (Wang et al., 2017; Lu G et al.,2012), co-precipitation (Raj et al., 2022), and so on. We prepared pure and iron-doped stannic oxide nanomaterials samples. On nano-scale, TM-doped tin-oxide exhibits interesting properties arising from quantum confinement and microstructual features. Such quantum confinement in particles of sizes less than 10nm is usually observed (Kumari et al., 2022). In this work, we consider co-precipitation method of synthesis of tinoxide ($SnO_2$) doped with transition metal iron for DMS synthesis and study of structural and magnetic properties for spintronics application.

## 2. EXPERIMENTAL METHOD AND MATERIALS

### Samples

Chemicals of analytic grade were procured as in Table 1 and were used without a further purification. To prepare virgin sample of $SnO_2$, first 0.1M solution was prepared by dissolving 3.506 g of $SnCl_4.5\ H_2O$ in 100ml de-ionised water at room temperature. It was put on hot plate at $35^o$ C and aqueous Ammonia was added into it drop-by-drop with stirring until the white precipitate was obtained (with pH around 8). After 30 minutes of stirring, and filtration, the precipitate was rinsed several times with de-ionized water to remove unreacted chemicals and other impurities. The washed precipitate

was dried at 120°C for 5 hours followed by natural cooling to room temperature. Finally powdered product was collected. Next, doped samples were prepared as follows. For preparing $Sn_{0.98}Fe_{0.02}O_2$, first stock solutions were prepared by dissolving 3.4358 g of $SnCl_4.5H_2O$ in 100ml DI water and 0.0397g of $FeCl_2.4H_20$ in 100 ml DI water, at room temperature. The two solutions were then mixed in a flask and put on hot plate at 35°C with continuous magnetic stirring. Aqueous ammonia was added drop-by-drop until white precipitate was obtained. It was stirred for half an hour, and then filtered. Precipitate was rinsed several times by DI water and put in oven for drying at 120°C for 5 hours and subsequent cooling to room temperature. Powdered sample was thus collected. Similarly, $Sn_{1-x}$ $Fe_xO_2$, with x= 0.04, 0.06 and 0.08, were prepared. These five samples [S00, S02, S04, S06 and S08] were, then, characterized.

**Table 1: Chemicals**

| Chemicals | Purity (%) | Source |
|---|---|---|
| $SnCl_4.5H_2O$ | 98 | Sigma Aldrich |
| $FeCl_2.4H_2O$ | 99 | Sigma Aldrich |
| Aqueous ammonia | 25(w/w) | Rankem |

**Characterizations**

Samples were subject to x-rays diffraction experiment in machine RIGAKUMINIFLE X600, using copper- K-alpha radiation of wavelength 1.5406 angstrom. The scan rate used was 2 degree per minute in steps of 0.02degree.These patterns appear in Figures 1-5.

The magnetic characterizations were performed using vibrating sample magnetometer, VSM

## 3. RESULTS AND DISCUSSIONS

We used analysis> fitting> nonlinear curve fit> gauss to obtain the positions of the peaks, their intensity and full width at half the maximum intensity (FWHM). In case of pure sample, for example, the Gauss fit to plane (301) is shown in Figure-1. Table 2 gives the results (data rounded at second place after decimal point) of such analysis of XRD of all the samples appearing in Figures 1 through 5.

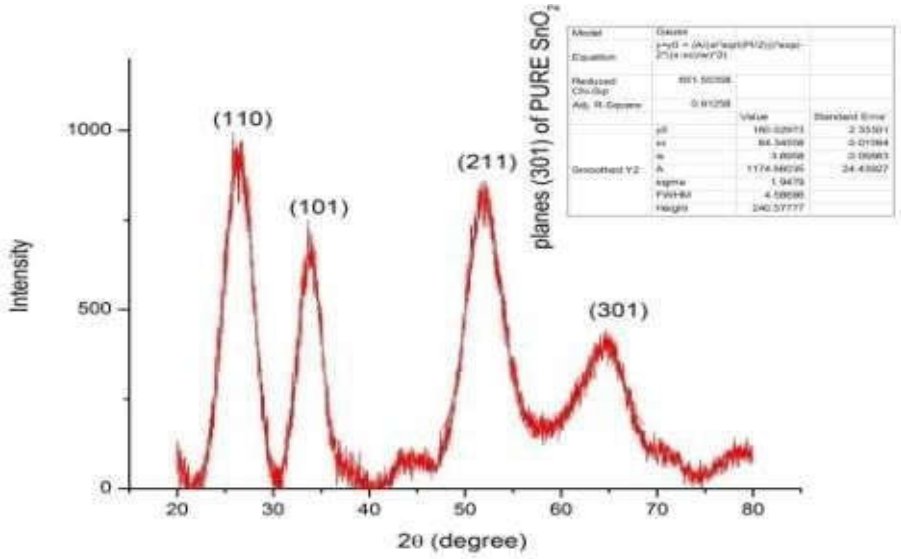


**Figure1: XRD analysis of peak for (301) of undoped SnO2**

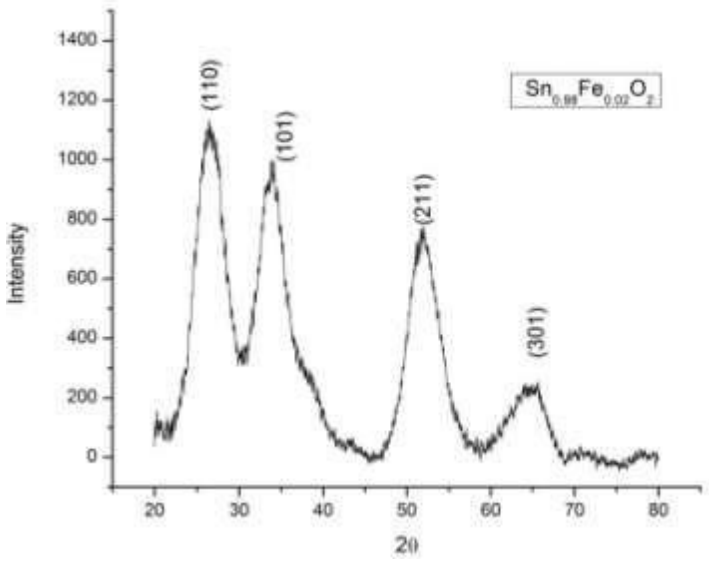


**Figure 2: XRD pattern of sample with 2% iron**

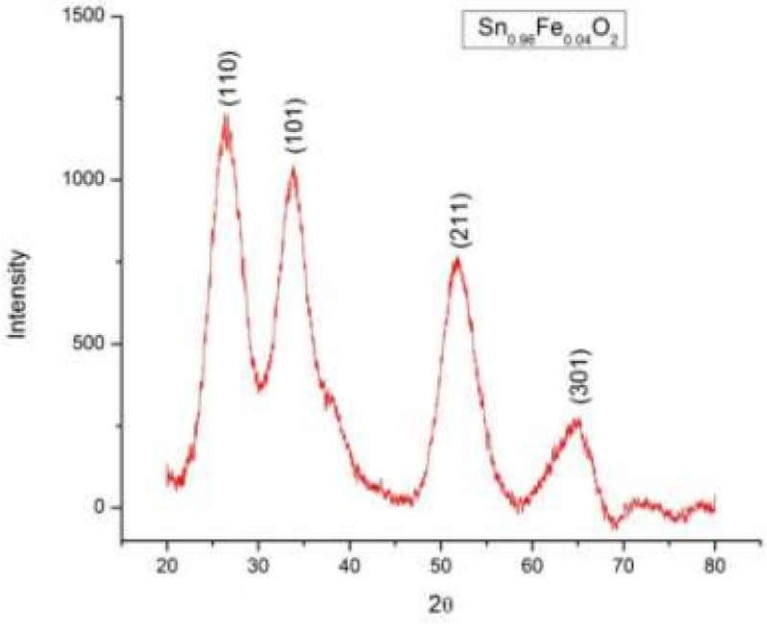


**Figure 3: XRD pattern of sample with 4% iron**

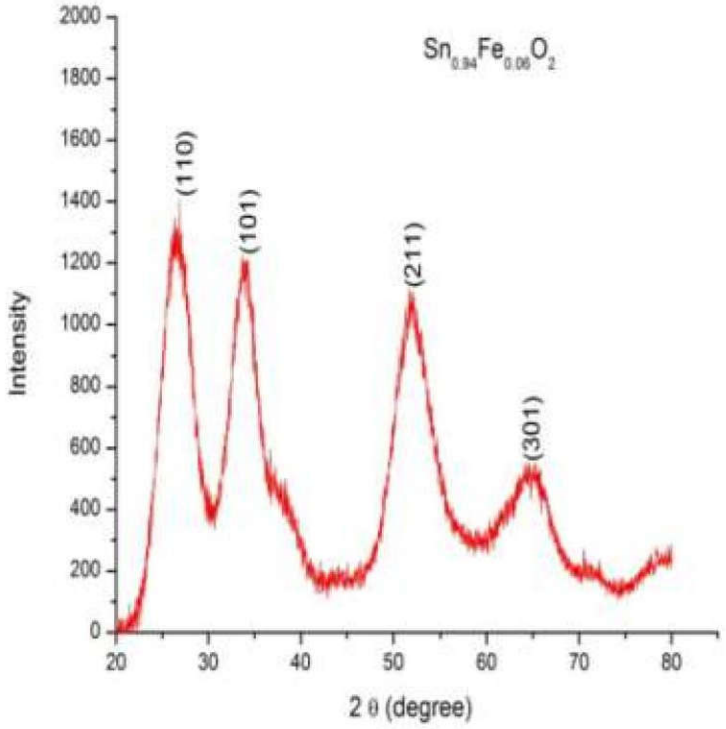


**Figure 4: XRD pattern of sample with 6% iron**

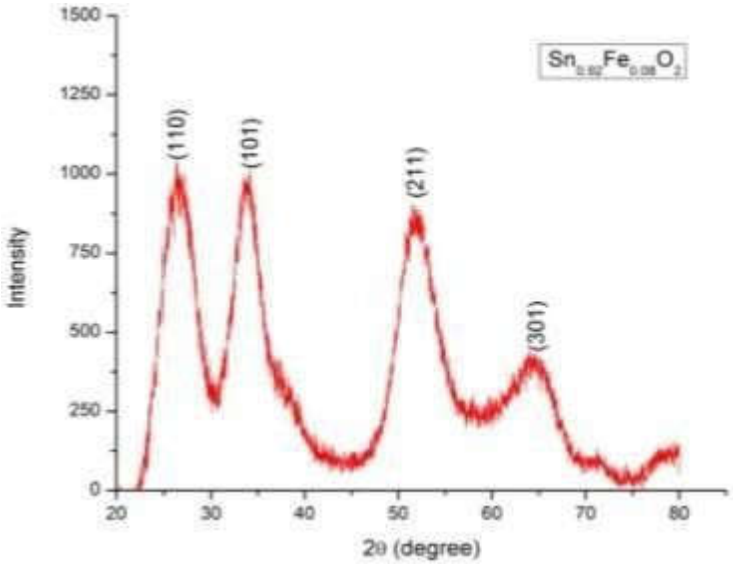


**Figure 5: XRD pattern of sample with8 % iron**

**Table 2: XRD pattern analysis**

| %Fe | (110) | | | (101) | | | (211) | | | (301) | | |
|---|---|---|---|---|---|---|---|---|---|---|---|---|
| | 2θ (°) | β (°) | Intensity | 2θ (°) | β (°) | Intensity | 2θ (°) | β (°) | Intensity | 2θ (°) | β (°) | Intensity |
| 0 | 26.39 | 3.75 | 950.44 | 33.83 | 2.95 | 639.69 | 52.05 | 4.19 | 671.96 | 64.34 | 4.59 | 240.57 |
| 2 | 26.61 | 4.23 | 1020.25 | 33.83 | 3.06 | 640.38 | 52.02 | 4.23 | 691.22 | 64.37 | 4.69 | 214.74 |
| 4 | 26.65 | 3.56 | 1018.90 | 33.88 | 2.97 | 786.36 | 52.09 | 4.07 | 745.09 | 64.25 | 5.53 | 292.62 |
| 6 | 26.71 | 4.45 | 1232.90 | 33.89 | 2.86 | 762.34 | 52.09 | 4.10 | 747.75 | 64.22 | 5.85 | 305.95 |
| 8 | 26.68 | 4.96 | 1084.75 | 33.86 | 2.92 | 645.79 | 52.12 | 4.78 | 705.09 | 63.66 | 8.92 | 515.95 |

The x-ray diffractions by samples show wide bases in their diffractograms whose origin is believed to be instrumental broadening and broadening due to nanometric crystallites in the samples. One is aware of Bragg's law for strong intensity of x-rays after diffraction by atoms in family of planes (hkl) in usual notations:

$$2d_{hkl}\sin\theta_{hkl}=\lambda \qquad (1)$$

$$\frac{1}{d_{hkl}^{\,2}}=\frac{h^2+k^2}{a^2}+\frac{l^2}{c^2} \qquad (2)$$

For (hkl) plane in tetragonal crystal system to which the patterns belong, the Bragg spacing is given by

The lattice parameters for the samples are found using x-ray pattern as in Table 3 for various concentration of dopant. These are consistent with JCPDS data file no. 41-1445, rutile (tetragonal) structure of symmetry space group P4 2/mnm, with lattice parameters $a$=0.47355 nm and c=0.31879 nm.

**Table 3: Lattice parameters: Variation with conc. of iron**

| Sample | $a$ (nm) | $c$(nm) |
|---|---|---|
| **S00** | 0.4772 | 0.3182 |
| **S02** | 0.4734 | 0.3194 |
| **S04** | 0.4727 | 0.3189 |
| **S06** | 0.4716 | 0.3191 |
| **S08** | **0.4721** | **0.3194** |

With increasing concentration of impurity atoms, there is, on the average, slight decrement in $a$ parameter. This is consistent with the size of dopant which is smaller than host atoms.

In a single in finite crystal with monochromatic x-rays incident as parallel beam, no broadening is expected. In practice, beams are not exactly parallel (instrumental effect) and beam cross section does illuminate a finite group of crystallites offering slightly different orientations of Bragg planes. These result in spreads in angles around centers of peaks. These spread depend on number of planes contributing to interference and are useful in determining crystallite sizes and strain in the crystallites. The mean crystallite size, or the average diameter D, in strain free system (Williamson & Hall, 1953) and no instrumental effect is given by Scherrer equation (Scherrer, 1918):

$$D=\frac{k\lambda}{\beta\cos\theta} \qquad (3)$$

Here k is shape factor, $\beta$ is full width at half the maximum (FWHM) of intensity of most intense

peak and $\theta$ is the half of the angular position of the centre of the peak in x-ray scan. In Table 2, FWHM for most intense peak(110), for example, increases with increasing dopant concentration, and angle also, so that particle size, determined by $\beta \cos \theta$ comes around 2 nm. This is illusory, however, because presence of strain and instrumental effects are usual in nanoparticles.

Nano crystallite sizes can be directly observed by TEM of high resolution or by indirect measurements. In the later case, XRD method and mercury porosity method can be included. In XRD pattern, peak broadening attributable to sample are crystallite sizes, micro strains, faulting and domain size distribution. In strumental broadening arises from slit width, sample penetration, deviation from monochromaticity of x-rays and imperfect focusing of beam. The two sources of broadening, size and instrumental, are analyzed on mathematical profile chosen; mainly Cauchy (Lorentzian profile) and Gauss (Gaussian profile) models are used. Additional line broadening due to micro strain $\varepsilon$ is considered by Stokes and Wilson (Stokes & Wilson, 1994)

$$\beta s = 4\,\epsilon \tan\theta \qquad (4)$$

Assuming linear additivity of broadenings (Cauchy), we get the equation

$$\beta \cos\theta = \frac{k\lambda}{D} + 4\epsilon \sin\theta \qquad (5)$$

Its plot is known as Williamson-Hall plot (Nye, 1985). These plots for the samples appear in figures 6(a) through 6(e); in figure 6(a), W-H plot for undoped sample S00 is shown.

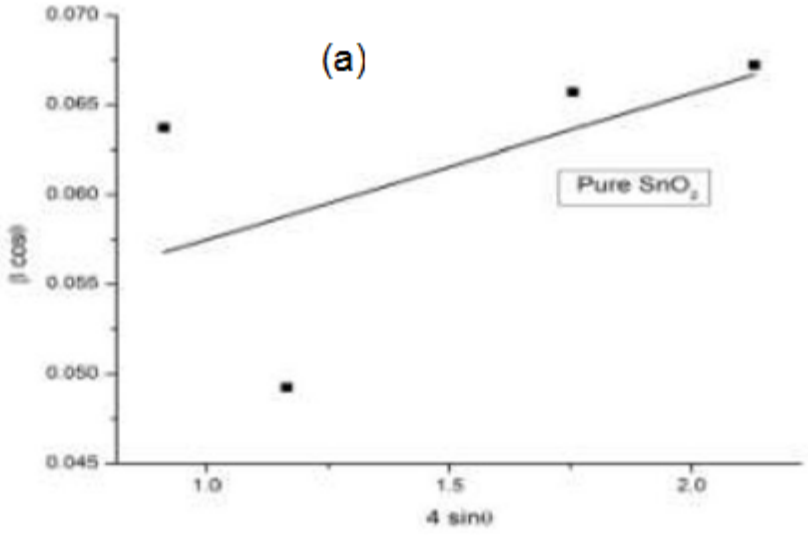


**Figure 6(a): W-HP lot forum doped sample (S00)**

The intercept of the plot was observed to be 0.04933 and slope 0.00815 having standard error reported as 0.01387 and 0.00886 respectively. The particle size calculated from the intercept and k=0.9, $\lambda$=1.5406 angstrom was found to be 2.8 nm. Similar plots for doped samples S02, S04, S06 and S08 were obtained and results were as tabulated (Table 4).

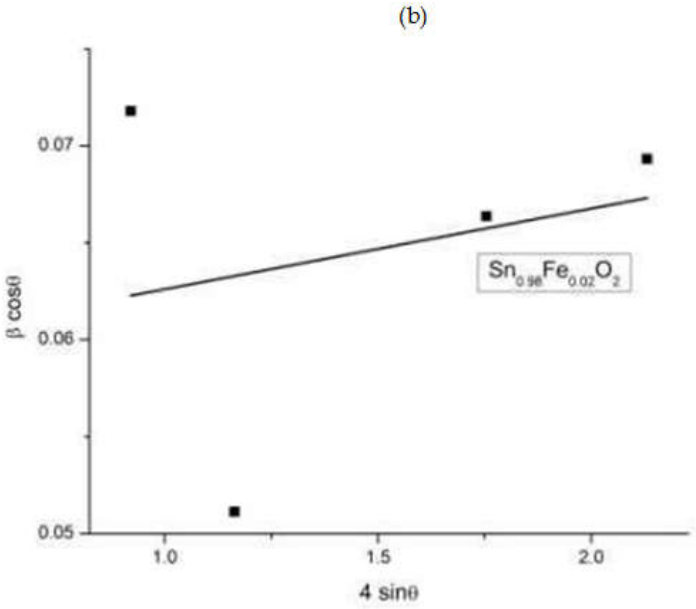
(b)
0.07
0.06
0.05
β cosθ
Sn0.98Fe0.02O2
1.0
1.5
2.0
4 sinθ

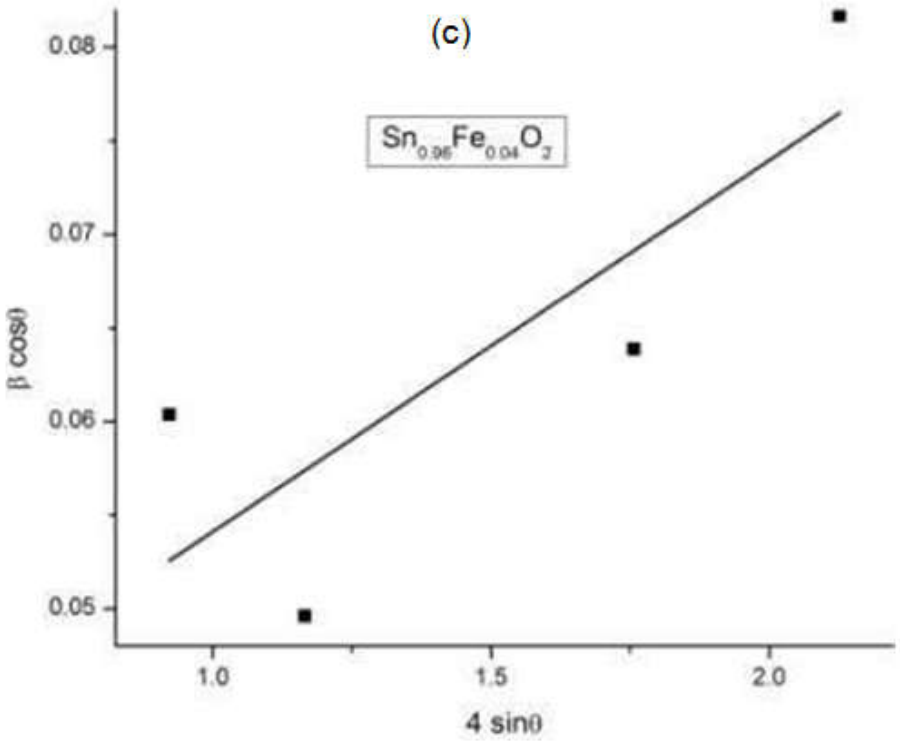
(c)
0.08
0.07
0.06
0.05
β cosθ
Sn0.96Fe0.04O2
1.0
1.5
2.0
4 sinθ

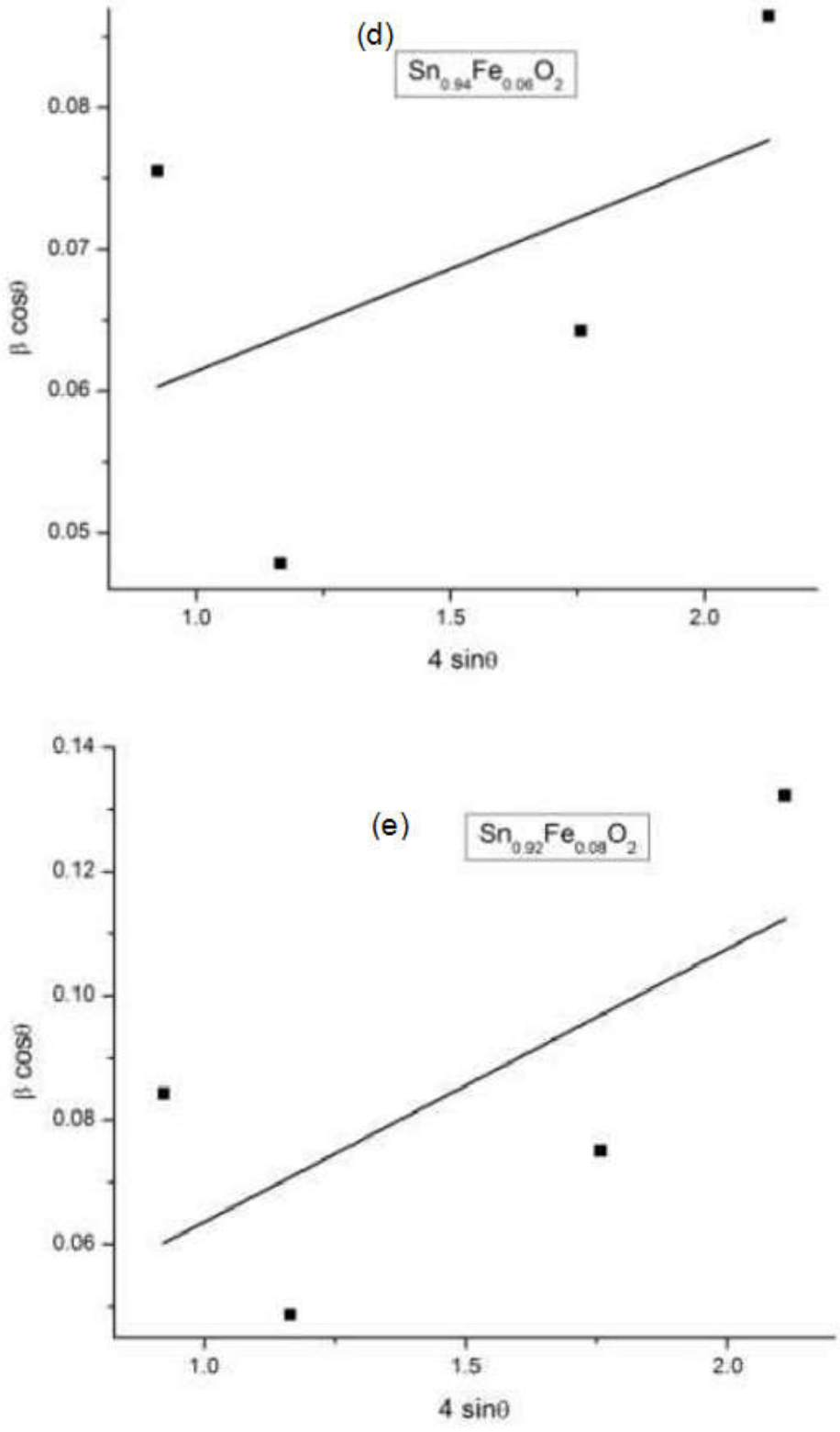


**Figure 6(b)-6(e): W-HP lots of dilute-doped samples S02, S04, S06 and S08**

**Table 4: Micro strain and mean particle size**

| Sample (Fefraction) | Particle size(W-H) nm | Micro strain (W-H) |
|---|---|---|
| **0.00** | 2.81 | 0.008 |
| **0.02** | 2.37 | 0.004 |
| **0.04** | 4.05 | 0.020 |
| **0.06** | 2.95 | 0.015 |
| **0.08** | 7.09 | 0.044 |

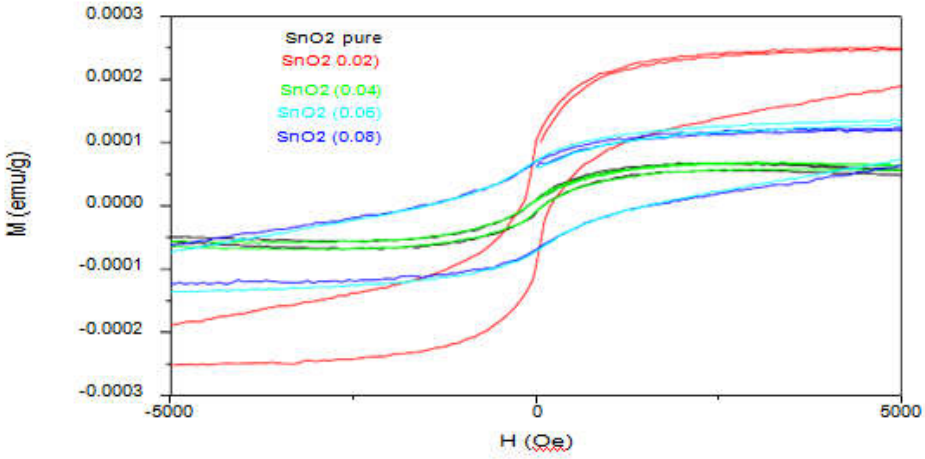


**Figure 7: FM in nano phase samples of Stannic dioxide host in 5kOe range**

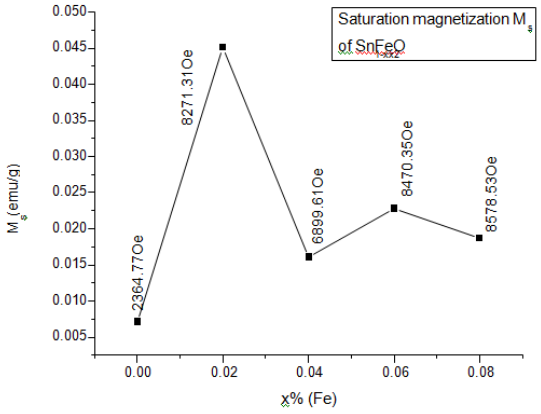


**Figure 8: Magnetization of samples at various impurity concentrations**

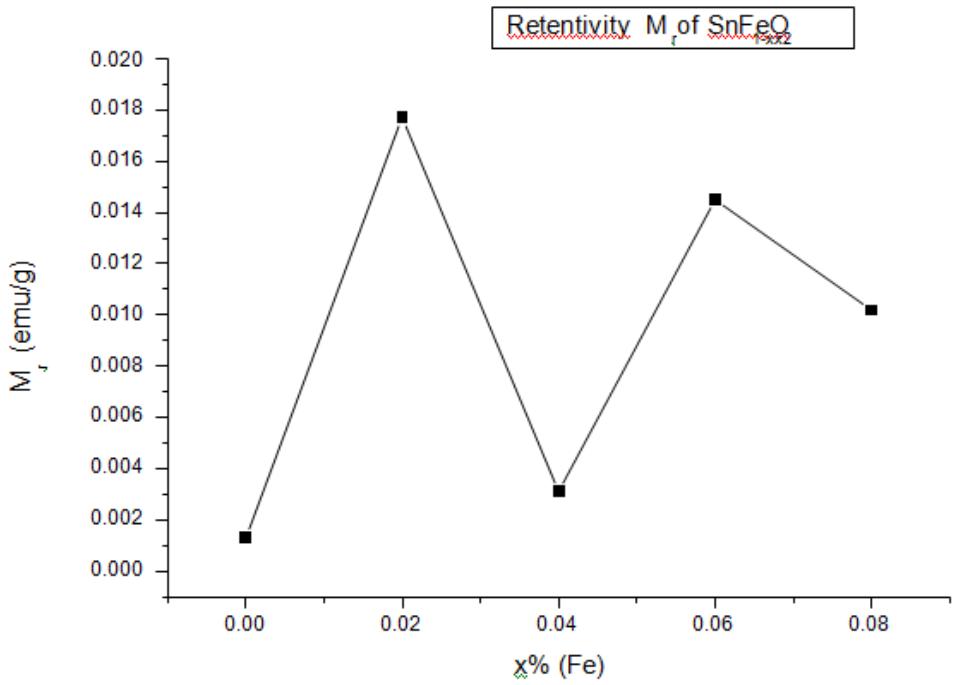


**Figure 9: Retentivity showing oscillatory increment**

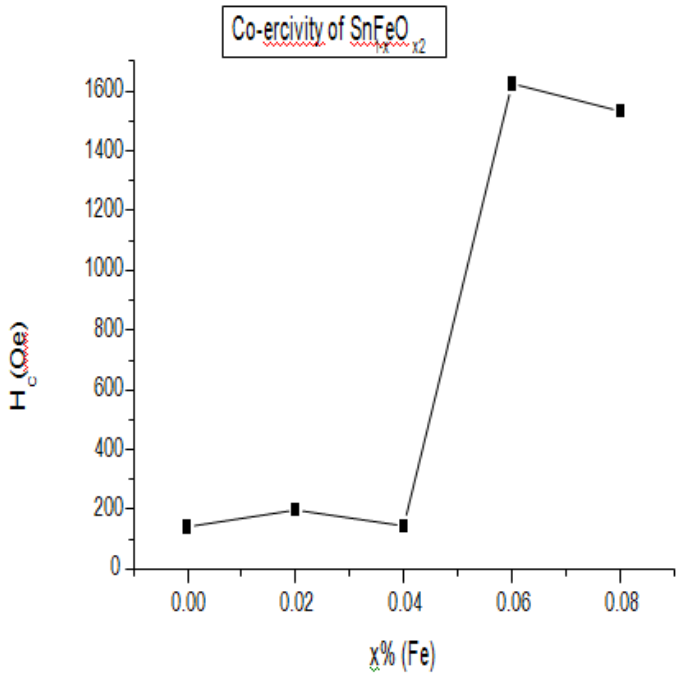


**Figure 10: Coercivity is maximum at x=0.06**

The numerical values of magnetic quantities are as in Table 5. The maximum magnetization is 0.044 emu/g. The existence of ferromagnetism in samples may have various origins like oxygen vacancies, sp-d interactions.

**Table 5: M-H curve Analysis**

| SAMPLEs | -Hc(Oe) | +Hc(Oe) | -Mr(emu/g) | +Mr(emu/g) | -Ms(emu/g) | +Ms(emu/g) |
|---|---|---|---|---|---|---|
| $SnO_2$(0.00) | -147.122458 | 142.795327 | -.0010608721 | 0.00106087211 | -0.0071188176 | 0.00717734855 |
| $SnO_2$(0.02) | -181.739507 | 216.356556 | -0.0176821773 | 0.0177875329 | -0.0449692713 | 0.0453555751 |
| $SnO_2$(0.04) | -147.122458 | X=142.795327 | -38.94418 | 38.94418 | -0.0156467662 | 0.0165422886 |
| $SnO_2$(0.06) | -1627.0013 | X=1622.67417 | -0.0144073749 | 0.014618086 | -0.0229236172 | 0.0226777875 |
| $SnO_2$(0.08) | -1518.82302 | 1549.11294 | -0.0102655838 | 0.0101997366 | -0.0188388938 | 0.0185491659 |

## 4. CONCLUSION

Nano materials particles of iron doped stannic oxide, $Sn_{1-x}$ $Fe_xO_2$, with x= 0.00, 0.02, 0.04, 0.06 and0.08, in sizes of around 3 nm were synthesized successfully by co-precipitation chemical method using room temperature and calcinations at 120°C. Observed lattice parameters were *a*=*b*=4.772 angstrom and c=3.182 angstrom, and size and micro strain using WH plots were found, respectively, nearly 3 nm and 4% in the nano particles. Only micro structural and magnetic properties are investigated in this work for different concentrations of dopantiron. The micro strain grows with increasing concentration of dopantiron. Size of dopant and its charge also seemingly influence the parameters. The maximum magnetization in low field of 5kOe range is observed to be 0.044 emu/g, and the ferromagnetic features render it suitable for spintronics applications.

## ACKNOWLEDGEMENT

Authors are thankful to Department of Physics, College of Commerce, Arts and Science, Patna, IIT, Patna, B. N. College, Patna and A. N. College, Patna for providing research facilities and fruitful discussions.

## REFERENCES

1. Bhagwat M., Shah P. & Ramaswamy V. (2003). Synthesis of nanocrystalline $SnO_2$ powder by amorphous citrate route. Materials Lett. 57, 1604-1611.
2. Calderon M.J. & Sarma SD. (2007). Theory of carrier mediated ferromagnetism in dilute magnetic oxides. Annals of physics 322, 2618.
3. Datta S and Das B. (1990). Electronic analog of the electro – opticmodulator. Appl. Phys. Lett. 56, 665- 667.
4. Diett T., Ohno H., Matsukura F., Cibert J. and Ferranol D. (2000), Zener model description of ferromagnetism in zinc blende magnetic semiconductors, Science, 287, 1019.
5. Fukumura T., Toyosaki H. & Yamada Y. (2005). Magnetic oxide semiconductors. Semicond. Sci. Teechnol. 20, 103.
6. Fujihara S. et al. (2004). Hydrothermal routes to prepare nano crystalline mesoporous $SnO_2$ having high thermal stability. A chem. Society, 20, 6476-6481.
7. Gnanam S. & Rajendram V. (2010). Luminescence properties of EG- Assisted $SnO_2$ Nanoparticles by Sol-gel process. Digest Journal of Nanomaterials and Biostructures, 5 699-704.
8. Hench L.L. & West J K. (1990). The Sol-gel process. Chem. Rev., 90, 33-72.
9. Janisch R., Gopal P. & Spaldin N.A. (2005). Transition metal – doped TiO2 and ZnO present status of the field, J. Phys. Condens. Matter, 17, 657.
10. Jungwirth T., Slinova J., Masek J., Mac Donald A.H. (2006). Theory of ferromagnetic (III, Mn) V semiconductors. Rev. Mod. Phys. 78, 809
11. Kumari N. et al. (2022). Microstructures and optical properties of PVA encapsulated cadmium selenide QD synthesized in non-stiochiometric ratio by green chemical route, Materials Today: Proceedings , 65(8), 3573-80.
12. Liu W. & Wang H. (2020). Flexible oxide epitaxial thin films for wearable electronics: fabrication physical properties and

applications. Journal of Materiomics, 6, 385-96.

**13.** Lu G. et al. (2006). Gas sensors based on tin oxide nanoparticles synthesized from a mini-arc plasma source. J. Nano materials, 1-7.

**14.** Li F. et al. (2002). One- step Solid- state reaction synthesis and gas sensing property of tin oxide nano particles. Sens. Actuators B, 81, 165-169.

**15.** Lu G et al. (2012). UV- enhanced room temperature NO2 sensor using ZnO nanorods modified with SnO2 nanoparticles. Sens. Actuators B: Chemical 162, 82-88.

**16.** Monalisa et al. (2021). Correlation between lattice strain and magnetic properties enhancement of nanocrystalline cobalt ferrite with controlled annealing. J .Matter sci: Mater Electron, 32, 23843-23853.

**17.** Matsumoto Y. et al. (2001). Room temperature ferromagnetism in transparent transition metal – doped titanium dioxide Science 291, 854.

**18.** Moore E.G. (1965). Cramming more components onto Integrated Circuits. Electronics magazine, 38(8).

**19.** Munekata H., Ohno H., Molnar Von., Segmaller A., Chang L.L. and Esaki L., (1989). Diluted magnetic III-V semiconductors. Phys. Rev. Lett. 63, 1849

**20.** Nye J F. (1985), Physical properties of crystals: Their Representation by Tensors and Matrices. Oxford New York.

**21.** Ohno H., (1998). Making nano magnetic semiconductors ferromagnetic Science, 281,951

**22.** Ohno H., Munekata H., Penney T., Molnar S von., Chang L.L. (1992). Magnetotransport properties of p type (In,Mn)As diluted magnetic III-V semiconductors. Phys. Rev. Lett. 68, 2664.

**23.** Ogale S.B. et al. (2003). High temperature ferromagnetism with a Giant Magnetic Moment in Transparent Co-doped $SnO_2$.. Phys. Rev. Lett. 91, 077205.

**24.** Raj R. et al. (2022)., Physical properties of quantum dot cadmium sulphide nano materials for its applications, prepared by low cost chemical method, Materials Today: proceedings, 66(4), 1750-55.

**25.** Rai B. C., Kumar S., Raj R., Kumari N., Monalisa et al.,(2016). Meso Spin-crystallites for new Electronics. SOJ Mater Sci Eng 4(1): 1-5.

**26.** Sasaki T., Sonoda S., Yamamoto Y., Suga Ken-ichi., Shimizu S., Kindo K. and Hori H. (2002). Magnetic and transport characteristics on high curie temperature ferromagnet of Mn – doped GaN., J. Appl. Phys., 91, 7911.

**27.** Sahm T, Madler L, Gurlo A, Barsan N, Pratsinis S.E., Weimar U. (2004). Flame spray synthesis of tin dioxide nano particles for gas sensing, Sens. Actuators B 98, 148–153.

**28.** Shaikh F. et al. (2018). Facile Co-precipitation synthesis and ethanol sensing performance of pd loaded Sr doped SnO2 nanoparticles. Powder Technol. 326, 479-87.

**29.** Scherrer. P. (1918), Nachrichten von der Gesselschaft der Wissenschaftenzu Gottingen, Mathematisch- Physikalische Klasse. 2, 98.

**30.** Stokes A.R and Wilson A J C. (1994). The diffraction of X-rays by distorted crystal aggregates-I, Proc. Phys. Soc. 56, 174.

**31.** Ueda K., Tabata H. & Kawai T. (2001), Magnetic and electric properties of transition metal -doped ZnO films. Appl. Phys. Lett. 79, 9.

**32.** Wang L P. et al. (2017). Novel Preparation of N-doped SnO2 Nanoparticles via Lasser – Assisted Pyrolysis: Demonstration of Exceptional Lithium Storage properties, Adv. Mater. 29(6), 1603286.

**33.** Williamson G K. & Hall H K. (1953). X-ray line broadening from field aluminium and wolfram, Acta. Metall, 1, 22-31.

**34.** Zutic I., Fabian J. and Sarma Das S. (2004). Spintronics: Fundamentals and applications, Rev. Mod. Phys. 76, 323.

**********